ACS APPLIED MATERIALS & INTERFACES

Research Article

www.acsami.org

Improved Efficiency of Hybrid Organic Photovoltaics by Pulsed Laser Sintering of Silver Nanowire Network Transparent Electrode

Joshua A. Spechler,[†] Ken A. Nagamatsu,[‡] James C. Sturm,[‡] and Craig B. Arnold*,[†]

[†]Department of Mechanical & Aerospace Engineering, Princeton University, Princeton, New Jersey United States

[‡]Department of Electrical Engineering, Princeton University, Princeton, New Jersey United States

ABSTRACT: In this Research Article, we demonstrate pulsed laser processing of a silver nanowire network transparent conductor on top of an otherwise complete solar cell. The macroscopic pulsed laser irradiation serves to sinter nanowire-nanowire junctions on the nanoscale, leading to a much more conductive electrode. We fabricate hybrid silicon/organic heterojunction photovoltaic devices, which have ITO-free, solution processed, and laser processed transparent electrodes. Furthermore, devices which have high resistive losses show up to a 35% increase in power conversion efficiency after laser processing. We perform this study over a range of laser fluences, and a range of nanowire area coverage to investigate the sintering mechanism of nanowires inside of a device stack. The increase in device performance is modeled using a simple photovoltaic diode approach and compares favorably to the experimental data.

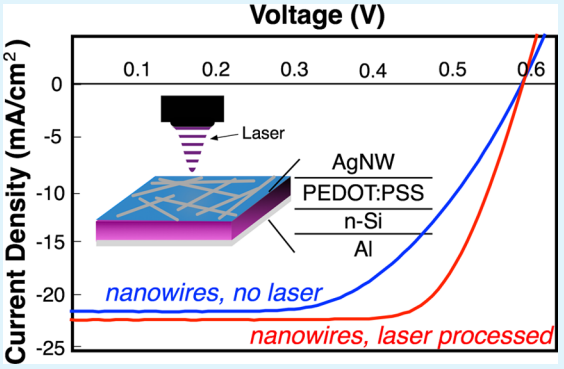

KEYWORDS: *transparent electrode, inorganic−organic heterojunction solar cell, nanowire network, direct laser sintering, solution processing*

INTRODUCTION

Percolating networks of silver nanowires (AgNW) efficiently conduct electricity while allowing optical radiation to pass with little absorption, leading to their use as transparent conducting electrodes.[1] When compared with the commonly employed indium−tin--oxide (ITO), two advantages of AgNW networks are often cited. First, the AgNW network is mechanically robust and can be used in flexible devices where ITO is inherently brittle.[2] Second, AgNW network electrodes are typically deposited in the laboratory atmosphere via spray coating, spin coating, or drop casting whereas ITO is typically sputtered onto a substrate in a high vacuum process.[3,4] This makes silver nanowires amenable to "roll-to-roll" production, which is impossible for ITO in many device settings.[5]

Currently, there is much active research on "post-processing" of AgNW network electrodes. This postprocessing decreases the sheet resistance of the resultant electrode by increasing the contact area at the narrow nanowire-to-nanowire junctions and by eliminating any residue, which may be on the AgNW surface from the synthesis.[6] A common method of postprocessing is a furnace anneal, which usually requires a temperature of 100−200 °C and a time on the order of an hour.[7,8] This process is both time-consuming and not ideal for nanowires on temperature sensitive substrates. Mechanical postprocessing of nanowire networks is another effective method, where the network electrode is treated with a mechanical stress on the order of megapascals.[9,10] This method is scalable and quick, however it may be damaging if the nanowire network is deposited directly onto an optoelectronic device, as this mechanical stress can easily deform thin polymer layers, or textured substrates.

Optical postprocessing methods sinters the nanowires together like a furnace anneal, and are expeditious and scalable like mechanical postprocessing. Many optical sources have been shown to efficiently weld nanowire junctions, such as pulsed lasers,[11] halogen lamps,[12] and high intensity pulsed lamps.[13−15] The halogen lamp and high intensity pulsed lamps are mainly absorbed around 355 nm, which is why a laser is preferable when unwanted absorption is to be avoided. Thus, the main advantage of using a laser is the wavelength can be tuned to this plasmonic absorption resonance targeting the energy to the junctions, and not the length of silver nanowires, or underlying layers. These previous studies focus on characterizing the optical postprocessing on ideal, thermally robust organic and inorganic substrates. Furthermore, no previous study has demonstrated optical postprocessing on poly(3,4-ethylenedioxythiophene) polystyrenesulfonate (PEDOT:PSS), a very common hole-transporting polymer which is often paired with AgNW electrodes in the literature.[16−20] In this paper, we use pulsed laser irradiation to sinter AgNW network electrodes on an otherwise complete PEDOT:PSS/n-Si photovoltaic device. We show that laser processing does not damage the device, and measure beneficial changes as compared to devices that do not undergo laser postprocessing.

Received: March 12, 2015
Accepted: April 27, 2015
Published: April 27, 2015

DOI: 10.1021/acsami.5b02203
ACS Appl. Mater. Interfaces 2015, 7, 10556−10562

We fabricate a hybrid organic PEDOT:PSS/n-silicon heterojunction cell, a device that has been extensively researched.[21−26] This device requires no high temperature n+ or p+ diffusion processing steps (typically >1000 °C) or plasma deposition processes that are typically used for high-efficiency crystalline silicon solar cells.[27,28] Furthermore, this device has shown promising results with AgNW network electrodes. Chen et. al[29] use a spin coated AgNW network, with no postprocessing, as a top electrode with textured silicon and PEDOT:PSS sublayers, they report a maximum power conversion efficiency of 10.1%. Khatri et. al[30] prepared AgNW network electrodes on glass, separately from a nontextured device stack. Those electrodes underwent a furnace anneal postprocessing of 200 °C for 20 min and they obtain a maximum power conversion efficiency of 9.7% after integration. Recently, Xu et. al[31] demonstrated this hybrid organic photovoltaic device with PCE of 13.3% when using graphene oxide as a conductive additive over a silver nanowire network. This result comes with the addition of another material into the stack, while we aim to refine the materials already defined. In this study, we directly deposit our nanowires onto the nontextured device, and use laser irradiation to postprocess the nanowire network. We observe that the devices are unharmed by the laser processing, due to the plasmonic mediated localization of the heating. Furthermore, devices that initially have poorly conducting top electrodes experience as much as a 35% increase in power conversion efficiency from this process. While the maximum absolute efficiency reported here, 9.2% is lower than the most recent values, this is likely due to a lack of short circuit current coming from two major sources: a lack of optimization of the thickness of our PEDOT:PSS layer, and the lack of any light trapping schemes such as texturing of the silicon wafer. However, the process described here, leading to the increases in the efficiency are generalizable to these higher current density devices.

EXPERIMENTAL DETAILS

Fabrication of the Solar Devices. Devices were fabricated on n-type float-zone silicon doped with phosphorus to a level of 2×10^{15} cm^{-3} as well as n-type Czochralski silicon doped with phosphorus to a level of 2×10^{16} cm^{-3}. PEDOT:PSS was purchased as CLEVIOS PH1000 (1.5% solids in H_20) from Baytron chemicals and 10%w/w Dimethyl Sulfoxide was added to enhance conductivity, as well as 0.25% Zonyl FS-300 surfactant to promote adhesion onto H-passivated silicon. Fabrication of all devices began with a standard RCA clean of the 16 mm × 16 mm silicon substrate. This is followed by a dip in 20:1 deionized water to hydrofluoric acid (HF), in order to remove any native oxide on the surface of the silicon. PEDOT:PSS was spun onto H-passivated silicon at 4000 rpm to form a 70 nm thick layer. The bottom metal electrode, and top contact bus-bar are deposited by thermal evaporation in a vacuum chamber with base pressure of 10^{-7} mbar. The sample is then scribed into 9 electrically isolated devices with 4 mm × 4 mm physical dimension.

Fabrication of the AgNW/PEDOT:PSS Electrodes. Cleaned 1 × 1 in. glass microscope slides were coated with PEDOT:PSS and spun at 4000 rpm to obtain 70 nm thick layers. AgNWs from Blue Nano Inc. were dispersed in methanol at a concentration of 2 mg/mL. The PEDOT:PSS coated glass was placed on a motorized, heated bed at 65C which moved at 4m/min under a spray nozzle, the AgNW suspension was fed to the nozzle at a rate of approximately 2 mL/min and sprayed via 35 psi nitrogen, eight passes under the nozzle produced the ∼10% area coverage electrode. A small (<2% area coverage) silver pad contact point is then thermally evaporated onto the sample for testing.

Measurement of the Solar Devices. Layer thicknesses were measured with a KLA-Tencor surface profilometer for the PEDOT:PSS films. Electrical characterization was carried out with an Agilent/Hewlett-Packard 4155c parameter analyzer. AM1.5G measurements were carried out using an OAI systems AAA Trisol solar simulator utilizing a 4 mmx4 mm aperture to ensure accurate photocurrent measurement. The power output of the solar simulator was measured using a silicon reference solar cell from PV Measurements Inc., which was calibrated by Newport Corporation PV Cell Lab.

Measurement of AgNW/PEDOT:PSS Electrodes. Sheet resistance measurements where achieved via 4-point measurements on small-evaporated silver contact points spaced 8 mm apart on top the AgNW network, with an Agilent/Hewlett-Packard 4155c parameter analyzer. Measurements were taken at 4 locations in the sample. The spectral transmission measurements and the diffuse (scattering) transmission measurements were obtained in a Hitachi U-3410 recording spectrophotometer with an integrating sphere.

Laser Sintering Process. The laser used in this study is a Coherent AVIA: 355 nm diode pumped solid state Nd:YVO_4 laser, with 27 ns pulses. Herein the laser is focused through a 5× objective (NA = 0.13) where spot size is kept constant at 500 μm diameter, and each area of the sample receives 625 pulses. The laser is rastered using an XY translation stage at a speed of 1200 mm/min. For all experiments except where otherwise noted, we use a fluence of of 23.5 mJ/cm^2. When optimizing for fluence we change the laser energy via active Q-switching while leaving the spot size unchanged. Both the devices and the electrodes on glass underwent the laser irradiation in air.

RESULTS AND DISCUSSION

The device fabrication, shown in Figure 1 begins with PEDOT:PSS deposited via spin coating onto a n-Si wafer. In the absence of a AgNW network electrode such a device would typically use a thermally evaporated busbar-and-finger style electrode, which would have a branching structure, where the spacing and size of the finger electrodes are designed to mitigate lateral resistance and shadowing. In this study the transparent electrode is fabricated by spray coating a AgNW suspension in the laboratory atmosphere (Figure 1b), resulting in a percolating layer of randomly oriented nanowires. The area coverage of the network depends on the number of spray coating passes, and presents a similar trade-off between shadowing and sheet resistance of the network. The nanowires used are purchased from Blue Nano Inc. and have a mean length of 15 μm and mean diameter of 90 nm. After the nanowire layer is spray coated onto the device, a small (100 μm × 3 mm, 2% area coverage) silver bus-bar is evaporated to serve

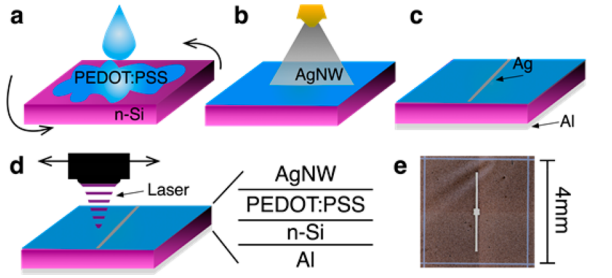

Figure 1. Schematic of the fabrication process for the hybrid organic PEDOT:PSS/n-Si heterojunction cell. (a) PEDOT:PSS is deposited onto n-Si via spin coating. (b) A coating of AgNW is spray coated on top of the PEDOT:PSS to serve as the transparent electrode. (c) A front contact bus-bar and back electrode are added via evaporation. (d) The AgNW network is laser processed in a raster fashion. (e) A photograph of the top side of a completed cell, showing the shape of the contact bus-bar.

DOI: 10.1021/acsami.5b02203
ACS Appl. Mater. Interfaces 2015, 7, 10556−10562

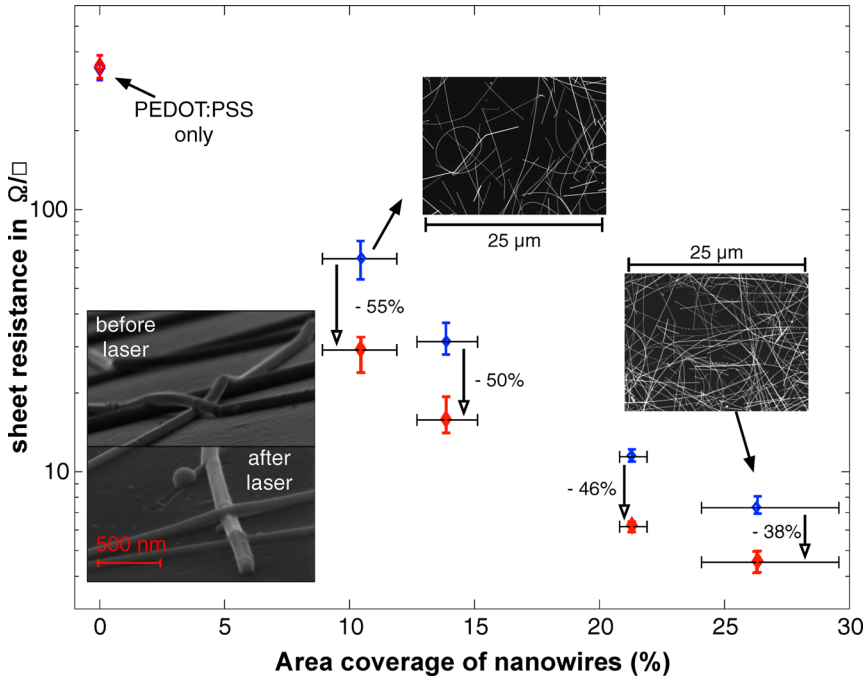

Figure 2. Sheet resistance before (blue symbols) and after (red symbols) laser processing of AgNW/PEDOT:PSS electrodes on glass as a function of the nanowire area coverage. The vertical error bars are min/max as the sheet resistance measurement was taken at 4 locations in the 1 in. square sample. The horizontal error bars are min/max and obtained via thresholding of 5 SEM images, sample images are inset in the plot. Additionally inset (lower left) is an SEM showing increased contact between nanowires as a result of laser processing.

as a testing contact point and the back contact is similarly formed in vacuum via blanket evaporation of aluminum (Figure 1c). The tops of the devices are then exposed to pulsed laser irradiation (Figure 1d). A completed device is shown in Figure 1e, to display the device dimensions and size of the electrical contact.

When integrated into the device stack, it is impossible to characterize the transparency or sheet resistance of the top electrode alone. Therefore, we also laser process AgNW networks on PEDOT:PSS coated glass slides and characterize them for changes in sheet resistance and optical transparency before and after laser irradiation. During deposition of the AgNW network, varying the number of passes under the spray coating nozzle varies the area coverage of the nanowires in the electrode, and therefore changes the initial sheet resistance. We can then estimate the area coverage of silver nanowires by image processing scanning electron micrograph (SEM) images. We take a large field of view 25 μm × 25 μm and use a thresholding method to count the fraction of the area covered by nanowires. A qualitative examination of the laser sintering can be observed in the large SEM micrograph inset in Figure 2, which shows increased contact between nanowires, as compared to the sample prior to optical processing.

The results shown in Figure 2 quantify the effect of laser sintering to the conductivity of the electrode. We observe reduction of sheet resistance after laser processing only when there are nanowires present. Additionally, the initial area coverage of the nanowire network is correlated to the amount of beneficial changes to the sheet resistance. That is, relative benefits (percent decrease in sheet resistance) from the laser processing are less when there is a higher amount of nanowires to begin with. This is qualitatively explained within the framework of the laser processing reducing the resistance at the junctions in the network. The laser processing reduces the resistance at junctions between nanowires. In dense nanowire networks, there are more junction points, acting in parallel. because these junctions act in parallel, the effective resistance of the junctions on the dense network is lower. Therefore, the reduction in junction resistance due to the laser has a smaller effect. In a high area coverage network (as in the 26% coverage network, shown) there are many high resistance junction points but they act in parallel - effectively making the network more conductive initially, thus after laser welding the AgNW/PEDOS:PSS electrode only shows a 38% decrease in sheet resistance. Whereas, in the lower, 10% area coverage network, we see a 55% decrease in sheet resistance after laser processing. It is also important to note that the data point at 0% area coverage, which is the PEDOT:PSS/glass electrode, shows no change in sheet resistance after laser processing.

Our previous study[11] showed the laser irradiation has no effect upon transparency when the nanowires are on a glass substrate, we observe this still holds for a PEDOT:PSS substrate. Figure 3 shows the postlaser-sintered specular transparency, and "total transparency", which is measured with an integrating sphere to include forward scattered light. The nanowires are efficient scatterers of light, as the "haze", measured as the ratio of diffuse to specular transmission, increases with area coverage. It has been reported that this haze is beneficial to photovoltaic devices, as it acts to frustrate spectral reflections from the surface, which would otherwise be lost illumination.[32,33] We thus report the total transmission, inclusive of haze as the relevant optical metric for the AgNW transparent conductor when used in a photovoltaic device. Inset in Figure 3 are raw total transmission spectra as a function of wavelength for (1) the 26% coverage electrode, (2) a similarly dense coating of nanowires with no PEDOT:PSS and no laser treatment, and (3) a sample with PEDOT:PSS only, for comparison. The spectrum of the 26% area coverage

DOI: 10.1021/acsami.5b02203
ACS Appl. Mater. Interfaces 2015, 7, 10556−10562

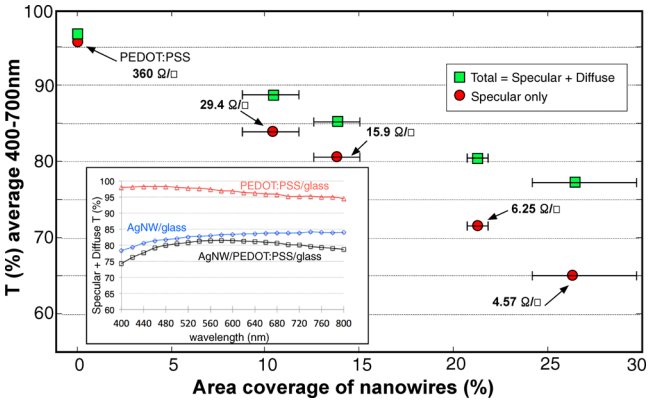

Figure 3. Averaged optical transmission (400 nm -700 nm) of the AgNW/PEDOT:PSS/glass electrodes as a function of the nanowire area coverage after laser processing. The sheet resistance numbers shown are those after the laser sintering from Figure 2. The horizontal error bars are the same as from Figure 2. Inset are sample spectrum through the visible (400−800 nm) comparing the PEDOT:PSS/glass, AgNW/glass, and AgNW/PEDOT:PSS/glass electrodes for 26% nanowire coverage. All the values have the glass substrate subtracted.

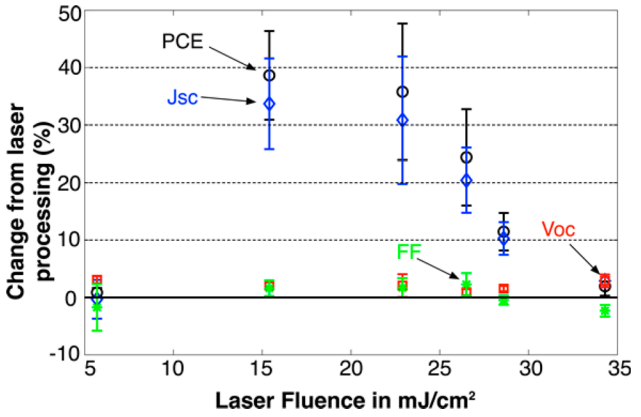

Figure 4. Change in device parameters (PCE, V_{OC}, J_{SC}, FF) as a function of the laser processing fluence. The error bars are ± one standard deviation from 8 samples. For this study a purposefully highly resistive (and therefore, poor absolute performance) electrode was used.

electrode is featureless, which is desirable for transparency, however a slight roll-off is seen at the UV side from an absorptive resonance in the silver nanowires (centered at about 360 nm) and a roll-off in the PEDOT:PSS at the IR side from the plasma frequency cutoff typically around 1 μm.[34] These tests upon the electrode, prepared separately from the device, serve not only to tune the nanowire network density variable but also to verify the PEDOT:PSS survives the laser irradiation without adverse effects to the polymer layer's conductivity or transparency.

To optimize the laser fluence for sintering the nanowires in the network electrode on top of a completed device stack (AgNW/PEDOT:PSS/n-Si/Al) we fabricate devices with a purposefully sparse coating of nanowires. We measure from thresholding SEM images of the device the nanowire area coverage is 6% ± 1%. As demonstrated in Figure 2, the sparser the nanowire network the more dramatic the effect of laser processing. We expect the sheet resistance of the top electrode to be >100 Ω/sq initially and decrease by more than 50% after laser processing. We fabricate seven sets of eight devices. We process the devices over a range of laser fluences (energy per area) while keeping the number of pulses constant. The spot size and number of pulses is the same as in the above process on the electrode alone, and the energy is changed via active Q-switching. The device receives laser irradiation in the laboratory atmosphere with silver nanowires as the top layer and the otherwise completed stack (PEDOT:PSS/n-Si/Al) as the effective substrate. The devices are tested before and after laser processing to extract relative changes to performance metrics: power conversion efficiency (PCE), open-circuit voltage (V_{OC}), short-circuit current (J_{SC}), and fill factor (FF). We can plot the results of this test on what we will term the "low" nanowire density in Figure 4.

This testing reveals that the optimal processing condition is roughly 20−25 mJ/cm^2. As noted, while the relative change to power conversion efficiency looks quite impressive in Figure 4, the poorly conducting (high sheet resistance) nanowire network layer gives rise to poor absolute device metrics.

Knowing the optimal conditions for laser processing, we now increase the area fraction of nanowires to produce devices with better absolute performance. We prepare two additional device batches to complement (what we will hereafter refer to as) the "low" area coverage devices used in the laser fluence optimization experiment. First, a device with "medium" nanowire area coverage, measured to have an area fraction of 16% ± 2%, and a device with "high" nanowire area coverage measured to be 25% ± 3%. We present relevant device metrics of the three batches in Table 1, and also single out the device, which shows the maximal PCE change. For the device with maximal PCE change, we show in Figure 5, the $J-V$ characteristics under AM1.5 illumination. In all three batches, we see beneficial changes to device metrics after the laser processing technique. Again, the device metrics presented here are for the same device before and after laser processing in the laboratory atmosphere, this is not a comparison between batches that are and are not laser processed. We conduct the experiment this way as to not involve any possibly unoptimized variables in our device manufacturing scheme.

We note that for a given device, depositing and processing nanowires should not be expected to change open-circuit voltage (V_{OC}), since the nanowires should predominantly affect the series resistance. We see that the open circuit voltage, while slightly different from batch to batch is mostly unchanged by the laser processing. The batch-to-batch differences in the open circuit voltages are expected from changing the dopant level (from 10^{16} cm^{-3} in the high batch to 10^{15} cm^{-3} in the medium and low batches). These batch-to-batch differences do not obscure the relative changes in performance due to the laser process. It is these relative changes which are telling of the importance of the laser processing upon the device.

It is also important to note that the device with the low nanowire area coverage (Figure 5a) experiences a 40% increase in short circuit current (J_{SC}), whereas the data set with "medium" nanowire area coverage(Figure 5b) shows no increase to the short circuit current. However, both of these batches show beneficial changes to the PCE. The medium batch gains to PCE seem to be only on account of the increase to fill factor (FF), as PCE = $V_{OC} \times J_{SC} \times$ FF. This result is can be qualitatively explained with a simple model of a solar cell with series resistance, R. The effect of the laser will be to decrease R in this circuit model, shown in Figure 6. Our model parameters (diode reverse saturation current, and photo generated current, I_{Photo}) can be anything we wish as long as

DOI: 10.1021/acsami.5b02203
ACS Appl. Mater. Interfaces 2015, 7, 10556−10562

Table 1. Parameters from the High, Medium, and Low Nanowire Coverage Batches[a]

	high: 25% coverage		medium: 16% coverage		low: 6% coverage	
nanowire coverage	before laser	after laser	before laser	after laser	before laser	after laser
PCE (%)	9.0 ± 0.1	9.0 ± 0.1	7.3 ± 0.4	9.2 ± 0.2	3.6 ± 0.9	5.0 ± 1.1
FF (%)	71 ± 1	69 ± 1	56 ± 3.4	66 ± 3.0	34 ± 2.2	35 ± 2.6
J_{SC} (mA/cm^2)	−20.4 ± 0.07	−20.8 ± 0.1	−22.4 ± 0.66	−23.7 ± 1.1	−17.8 ± 3.6	−23.5 ± 3.7
V_{OC} (V)	0.62 ± 0.001	0.63 ± 0.005	0.58 ± 0.004	0.59 ± 0.005	0.584 ± 0.001	0.59 ± 0.003
R_s (Ohm)	22.5	26.3	45.6	22.3	125	61.9

[a]Average and one standard deviation are given for a batch of 8 devices; additionally, the fit series resistance from Figure 5 is called out individually.

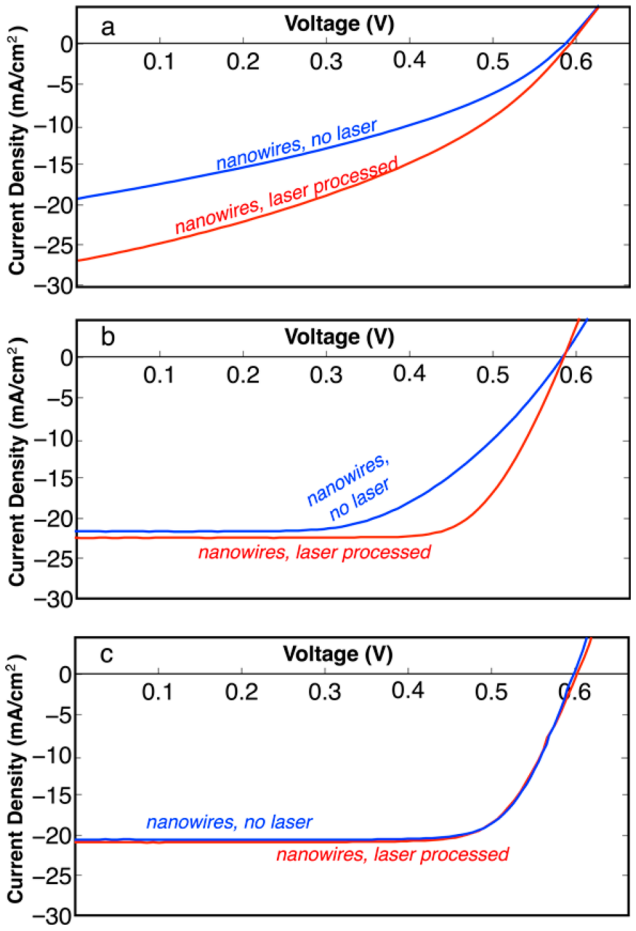

Figure 5. Results of laser processing the hybrid organic PEDOT:PSS/n-Si heterojunction cells. Shown are three different batches low, medium, and high initial nanowire area coverage (or density). $J-V$ characteristics under 1 sun (AM1.5) illumination for a single cell shown before laser processing, and after laser processing for the (a) low nanowire density, (b) medium nanowire density, where an additional curve before the nanowires are added is shown, and (c) high nanowire density.

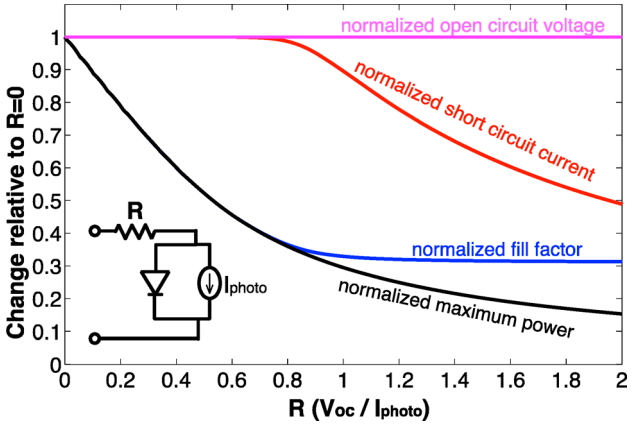

Figure 6. Plotted is the power output, V_{OC}, J_{SC}, and fill factor, normalized to the R = 0 value, for the circuit model of a solar cell (shown in inset) as a function of the series resistance R. The series resistance is varied from 0 to 2 V_{OC}/I_{Photo}. Note that the open circuit voltage is independent of R.

we examine the effect of series resistance in "natural units" of V_{OC}/I_{Photo}. We plot the J_{SC}, V_{OC}, FF, and PCE (normalized to the values at R = 0) as the resistance increases from 0 to 2 V_{OC}/I_{Photo}. We observe that changes to short circuit current are most dramatic when the series resistance is large (>0.8 V_{OC}/I_{Photo}), and changes to fill factor are more dramatic when the resistance is small (<0.8 V_{OC}/I_{Photo}). Physically, this occurs because at very large series resistances, the IV curve in the power-producing quadrant is dominated by R and becomes nearly a straight line, with slope $1/R$ and passing through the open circuit voltage point. The open circuit voltage point is unaffected by R, since at that point no current is flowing.

From the $J-V$ characteristics in Figure 5a–c, we can fit the simple circuit model to give us the series resistance value in Table 1, labeled R_s. One component of this series resistance is the sheet resistance of the AgNW transparent electrode. From the results shown in Figure 5 and Table 1 we approximate that the low device initially has a series resistance of 125 Ω which is about 1 V_{OC}/I_{Photo} (I_{photo}, we approximate to be 5 mA from extrapolating Figure 5a) for our device. This is in the range in which our simple model predicts the short circuit current should start showing increases with decreased series resistance. However, in the medium area coverage devices the prelaser series resistance is 0.4 V_{OC}/I_{Photo} that is why no increase to the short circuit current is observed when the series resistance is lowered. The high area coverage has a prelaser series resistance of 0.2 V_{OC}/I_{Photo} this already very low series resistance is the reason that the benefits of laser process are not observed in the device metrics. Further, we posit that the slight uptick in series resistance seen in the high nanowire area coverage device is not significant and is likely due to variations in the fitting for the series resistance variable. Interestingly both the high and the medium batches reach a final series resistance with similar absolute value, this is likely indicative that ∼25 Ω is comprised of the other elements of series resistance found in the device and testing setup.

CONCLUSIONS

We have demonstrated that laser sintering of a AgNW network transparent electrode is achievable on top of a completed device stack sublayer. The silicon hybrid organic hetero-

DOI: 10.1021/acsami.5b02203
ACS Appl. Mater. Interfaces 2015, 7, 10556–10562

junction, when laser processed shows marked improvements to the fill factor and short circuit current, which increase the power conversion efficiency of the device. Through examination of the electrode alone we characterized the effects of laser sintering the nanowires, and showed this gentle process leaves the PEDOT:PSS unchanged. The open circuit voltage of devices which are laser processed showed no change, meaning that the laser, while decreasing the total series resistance of the device did not alter the fundamental properties of the n-Si/PEDOT:PSS interface. The beneficial changes to the device are consistent with decreasing the series resistance, as illustrated by a simple circuit model. With the solution processed and laser postprocessed electrodes presented in this study we have shown how solution-processed nanowires and gentle laser processing are promising directions for low cost organic electronic manufacturing.

AUTHOR INFORMATION

Corresponding Author

*E-mail: cbarnold@princeton.edu.

Notes

The authors declare no competing financial interest.

ACKNOWLEDGMENTS

The authors would like to acknowledge the support of the National Science Foundation via the MRSEC at Princeton grant DMR-0819860 and the usage of the PRISM Imaging and Analysis Center. J.S. and C.B.A. acknowledge support from the Rutgers-Princeton NSF-IGERT on Nanotechnology for Clean Energy.

REFERENCES

(1) Hu, L.; Wu, H.; Cui, Y. Metal Nanogrids, Nanowires, and Nanofibers for Transparent Electrodes. *MRS Bull.* **2011**, *36*, 760−765.

(2) Langley, D.; Giusti, G.; Mayousse, C.; Celle, C.; Bellet, D.; Simonato, J.-P. Flexible Transparent Conductive Materials Based on Silver Nanowire Networks: A Review. *Nanotechnology* **2013**, *24*, 452001.

(3) Gordon, R. G. Criteria for Choosing Transparent Conductors. *MRS Bull.* **2000**, *25*, 52−57.

(4) Ginley, D. S.; Perkins, J. D. Transparent Conductors. In *Handbook of Transparent Conductors*; Ginley, D. S.; Hosono, H.; Paine, D. C., Eds.; Springer: New York, 2011; pp 1−25.

(5) Krebs, F. C.; Gevorgyan, S. a.; Alstrup, J. A Roll-to-Roll Process to Flexible Polymer Solar Cells: Model Studies, Manufacture and Operational Stability Studies. *J. Mater. Chem.* **2009**, *19*, 5442.

(6) Lee, J.-Y.; Connor, S. T.; Cui, Y.; Peumans, P. Solution-Processed Metal Nanowire Mesh Transparent Electrodes. *Nano Lett.* **2008**, *8*, 689−692.

(7) De, S.; Higgins, T. M.; Lyons, P. E.; Doherty, E. M.; Nirmalraj, P. N.; Blau, W. J.; Boland, J. J.; Coleman, J. N. Silver Nanowire Networks as Flexible, Transparent Conducting Films: Extremly High DC to Optical Conductivity Ratios. *ACS Nano* **2009**, *3*, 1767−1774.

(8) Langley, D. P.; Lagrange, M.; Giusti, G.; Jiménez, C.; Bréchet, Y.; Nguyen, N. D.; Bellet, D. Metallic Nanowire Networks: Effects of Thermal Annealing on Electrical Resistance. *Nanoscale* **2014**, *6*, 13535−13543.

(9) Tokuno, T.; Nogi, M.; Karakawa, M.; Jiu, J.; Nge, T. T.; Aso, Y.; Suganuma, K. Fabrication of Silver Nanowire Transparent Electrodes at Room Temperature. *Nano Res.* **2011**, *4*, 1215−1222.

(10) Yang, C.; Gu, H.; Lin, W.; Yuen, M. M.; Wong, C. P.; Xiong, M.; Gao, B. Silver Nanowires: From Scalable Synthesis to Recyclable Foldable Electronics. *Adv. Mater.* **2011**, *23*, 3052−3056.

(11) Spechler, J. A.; Arnold, C. B. Direct-Write Pulsed Laser Processed Silver Nanowire Networks for Transparent Conducting Electrodes. *Appl. Phys. A: Mater. Sci. Process.* **2012**, *108*, 25−28.

(12) Garnett, E. C.; Cai, W.; Cha, J. J.; Mahmood, F.; Connor, S. T.; Greyson Christoforo, M.; Cui, Y.; McGehee, M. D.; Brongersma, M. L. Self-Limited Plasmonic Welding of Silver Nanowire Junctions. *Nat. Mater.* **2012**, *11*, 241−249.

(13) Jiu, J.; Sugahara, T.; Nogi, M.; Araki, T.; Suganuma, K.; Uchida, H.; Shinozaki, K. High-Intensity Pulse Light Sintering of Silver Nanowire Transparent Films on Polymer Substrates: The Effect of the Thermal Properties of Substrates on the Performance of Silver Films. *Nanoscale* **2013**, *5*, 11820−11828.

(14) Araki, T.; Jiu, J.; Nogi, M.; Koga, H.; Nagao, S.; Sugahara, T.; Suganuma, K. Low Haze Transparent Electrodes and Highly Conducting Air Dried Films with Ultra-Long Silver Nanowires Synthesized by One-Step Polyol Method. *Nano Res.* **2013**, *7*, 236−245.

(15) Li, R.; Hu, A.; Zhang, T.; Oakes, K. D. Direct Writing on Paper of Foldable Capacitive Touch Pads with Silver Nanowire Inks. *ACS Appl. Mater. Interfaces* **2014**, *6*, 21721−21729.

(16) Zhu, R.; Chung, C.-H.; Cha, K. C.; Yang, W.; Zheng, Y. B.; Zhou, H.; Song, T.-B.; Chen, C.-C.; Weiss, P. S.; Li, G.; Yang, Y. Fused Silver Nanowires with Metal Oxide Nanoparticles and Organic Polymers for Highly Transparent Conductors. *ACS Nano* **2011**, *5*, 9877−9882.

(17) Gaynor, W.; Hofmann, S.; Christoforo, M. G.; Sachse, C.; Mehra, S.; Salleo, A.; McGehee, M. D.; Gather, M. C.; Lüssem, B.; Müller-Meskamp, L.; Peumans, P.; Leo, K. Color in the Corners: ITO-Free White OLEDs with Angular Color Stability. *Adv. Mater.* **2013**, *25*, 4006−4013.

(18) Krantz, J.; Stubhan, T.; Richter, M.; Spallek, S.; Litzov, I.; Matt, G. J.; Spiecker, E.; Brabec, C. J. Spray-Coated Silver Nanowires as Top Electrode Layer in Semitransparent P3HT:PCBM-Based Organic Solar Cell Devices. *Adv. Funct. Mater.* **2013**, *23*, 1711−1717.

(19) Gaynor, W.; Burkhard, G. F.; McGehee, M. D.; Peumans, P. Smooth Nanowire/Polymer Composite Transparent Electrodes. *Adv. Mater.* **2011**, *23*, 2905−2910.

(20) Margulis, G. Y.; Christoforo, M. G.; Lam, D.; Beiley, Z. M.; Bowring, A. R.; Bailie, C. D.; Salleo, A.; McGehee, M. D. Spray Deposition of Silver Nanowire Electrodes for Semitransparent Solid-State Dye-Sensitized Solar Cells. *Adv. Energy Mater.* **2013**, *3*, 1657−1663.

(21) Wright, M.; Uddin, A. Organic—Inorganic Hybrid Solar Cells: A Comparative Review. *Sol. Energy Mater. Sol. Cells* **2012**, *107*, 87−111.

(22) Avasthi, S.; Lee, S.; Loo, Y.-L.; Sturm, J. C. Role of Majority and Minority Carrier Barriers Silicon/organic Hybrid Heterojunction Solar Cells. *Adv. Mater.* **2011**, *23*, 5762−5766.

(23) Nagamatsu, K. A.; Member, S.; Avasthi, S.; Jhaveri, J.; Sturm, J. C. A 12% Efficient Silicon/PEDOT: PSS Heterojunction Solar Cell Fabricated at <100 ∘ C. *IEEE J. Photovoltaics* **2014**, *4*, 260−264.

(24) Yu, P.; Tsai, C.-Y.; Chang, J.-K.; Lai, C.-C.; Chen, P.-H.; Lai, Y.-C.; Tsai, P.-T.; Li, M.-C.; Pan, H.-T.; Huang, Y.-Y.; Wu, C.-I.; Chueh, Y.-L.; Chen, S.-W.; Du, C.-H.; Horng, S.-F.; Meng, H.-F. 13% Efficiency Hybrid Organic/silicon-Nanowire Heterojunction Solar Cell via Interface Engineering. *ACS Nano* **2013**, *7*, 10780−10787.

(25) Fan, X.; Zhang, M.; Wang, X.; Yang, F.; Meng, X. Recent Progress in Organic−Inorganic Hybrid Solar Cells. *J. Mater. Chem. A* **2013**, *1*, 8694.

(26) Xia, Z.; Song, T.; Sun, J.; Lee, S.-T.; Sun, B. Plasmonic Enhancement in Hybrid organic/Si Heterojunction Solar Cells Enabled by Embedded Gold Nanoparticles. *Appl. Phys. Lett.* **2014**, *105*, No. 241110.

(27) Zhao, J.; Wang, A.; Green, M. A.; Ferrazza, F. 19.8% Efficient "Honeycomb" Textured Multicrystalline and 24.4% Monocrystalline Silicon Solar Cells. *Appl. Phys. Lett.* **1998**, *73*, 1991−1993.

(28) Yamaguchi, T.; Ichihashi, Y.; Mishima, T.; Matsubara, N.; Yamanishi, T. Achievement of More Than 25% Conversion Heterojunction Solar Cell. *IEEE J. Photovoltaics* **2014**, *4*, 1433−1435.

DOI: 10.1021/acsami.5b02203
ACS Appl. Mater. Interfaces 2015, 7, 10556−10562

(29) Chen, T.-G.; Huang, B.-Y.; Liu, H.-W.; Huang, Y.-Y.; Pan, H.-T.; Meng, H.-F.; Yu, P. Flexible Silver Nanowire Meshes for High-Efficiency Microtextured Organic−Silicon Hybrid Photovoltaics. *ACS Appl. Mater. Interfaces* **2012**, *4*, 6857−6864.
(30) Khatri, I.; Liu, Q.; Ishikawa, R.; Ueno, K.; Shirai, H. Self Assembled Silver Nanowire Mesh as Top Electrode for Organic−Inorganic Hybrid Solar Cell 1. *Can. J. Phys.* **2014**, *92*, 867−870.
(31) Xu, Q.; Song, T.; Cui, W.; Liu, Y.; Xu, W.; Lee, S.-T.; Sun, B. Solution-Processed Highly Conductive PEDOT:PSS/AgNW/GO Transparent Film for Efficient Organic-Si Hybrid Solar Cells. *ACS Appl. Mater. Interfaces* **2015**, *7*, 3272−3279.
(32) Chiba, Y.; Islam, A.; Komiya, R.; Koide, N.; Han, L. Conversion Efficiency of 10.8% by a Dye-Sensitized Solar Cell Using a TiO_2 Electrode with High Haze. *Appl. Phys. Lett.* **2006**, *88*, No. 223505.
(33) Fang, Z.; Zhu, H.; Yuan, Y.; Ha, D.; Zhu, S.; Preston, C.; Chen, Q.; Li, Y.; Han, X.; Lee, S.; Chen, G.; Li, T.; Munday, J.; Huang, J.; Hu, L. Novel Nanostructured Paper with Ultrahigh Transparency and Ultrahigh Haze for Solar Cells. *Nano Lett.* **2014**, *14*, 765−773.
(34) Elschner, A.; Kirchmeyer, S.; Lövenich, W.; Merker, U.; Reuter, K. *PEDOT: Principles and Applications of an Intrinsically Conductive Polymer*; CRC Press: Boca Raton, FL, 2010; pp 136−143.

DOI: 10.1021/acsami.5b02203
ACS Appl. Mater. Interfaces 2015, 7, 10556−10562